

Transiting exoplanets from the CoRoT space mission [★]

XVI. CoRoT-13b: a dense hot Jupiter in transit around a star with solar metallicity and super-solar lithium content

J. Cabrera^{1,2}, H. Bruntt³, M. Ollivier⁴, R. F. Díaz⁵, Sz. Csizmadia¹, S. Aigrain⁶, R. Alonso⁷, J.-M. Almenara⁸, M. Auvergne³, A. Baglin³, P. Barge⁹, A. S. Bonomo⁹, P. Bordé⁴, F. Bouchy^{10,5}, L. Carone¹¹, S. Carpano¹², M. Deleuil⁹, H. J. Deeg⁸, R. Dvorak¹³, A. Erikson¹, S. Ferraz-Mello¹⁴, M. Fridlund¹², D. Gandolfi^{15,12}, J.-C. Gazzano^{9,16}, M. Gillon^{7,17}, E. W. Guenther¹⁵, T. Guillot¹⁶, A. Hatzes¹⁵, M. Havel¹⁶, G. Hébrard⁵, L. Jorda⁹, A. Léger⁴, A. Llebaria⁹, H. Lammer¹⁸, C. Lovis⁷, T. Mazeh¹⁹, C. Moutou⁹, P. von Paris¹, M. Pätzold¹¹, D. Queloz⁷, H. Rauer^{1,20}, D. Rouan³, A. Santerne⁹, J. Schneider², B. Tingley⁸, R. Titz-Weider¹, and G. Wuchterl¹⁵

(Affiliations can be found after the references)

Received ; accepted

ABSTRACT

We announce the discovery of the transiting planet CoRoT-13b. Ground based follow-up in CFHT and IAC80 confirmed CoRoT's observations. The mass of the planet was measured with the HARPS spectrograph and the properties of the host star were obtained analyzing Keck data. It is a hot Jupiter-like planet with an orbital period of 4.04 days, 1.3 Jupiter masses, 0.9 Jupiter radii, and a density of 2.34 g cm^{-3} . It orbits a G0V star with $T_{\text{eff}} = 5945\text{K}$, $M_* = 1.09M_{\odot}$, $R_* = 1.01R_{\odot}$, solar metallicity, a lithium content of +1.45 dex, and an estimated age between 0.12 and 3.15 Gyr. The lithium abundance of the star is consistent with its effective temperature, activity level, and age range derived from the stellar analysis. The density of the planet is extreme for its mass. It implies the existence of an amount of heavy elements with a mass between about 140 and $300M_{\oplus}$.

Key words. stars: planetary systems - techniques: photometry - techniques: radial velocities - techniques: spectroscopic

[★] The CoRoT space mission, launched on December 27th 2006, has been developed and is operated by CNES, with the contribution of Austria, Belgium, Brazil, ESA (RSSD and Science Programme), Germany and Spain. Part of the observations were obtained at the Canada-France-Hawaii Telescope (CFHT) which is operated by the National Research Council of Canada, the Institut National des Sciences de l'Univers of the Centre National de la Recherche Scientifique of France, and the University of Hawaii. Based on observations made with HARPS spectrograph on the 3.6-m European Organisation for Astronomical Research in the Southern Hemisphere telescope at La Silla Observatory, Chile (ESO program 184.C-0639). Based on observations made with the IAC80 telescope operated on the island of Tenerife by the Instituto de Astrofísica de

1. Introduction

Transiting planets are fundamental objects for the understanding of planetary formation and evolution. Their particular geometrical orientation allows the simultaneous measurement of their mass and radius, permitting a first order study of their internal structure. Moreover, through the careful analysis of their passages in front of (primary transit) and behind (occultation of the planet or secondary transit) their host star, a characterization of the composition and the temperature structure of their atmosphere can be carried out.

CoRoT is a space telescope dedicated to the study of asteroseismology and the discovery of extrasolar planets by the method of transits (Baglin et al. 2006). The *CoRoT* survey has previously detected, among other planets, the faint signal of a small rocky planet (Léger, Rouan, Schneider et al. 2009; Queloz et al. 2009; Bruntt et al. 2010b) and a giant planet with a temperate surface temperature (Deeg et al. 2010).

This paper presents the discovery of the planet CoRoT-13b, a dense giant planet in a close orbit around a main sequence star. Section 2 describes the observations performed with the satellite. Ground based observations including spectroscopic characterization of the star and radial velocity measurements are reported in section 3. The derivation of the planetary parameters is described in section 4. A discussion of the results is presented in section 5.

2. CoRoT observations

The observations of the *CoRoT* field LRa02 started on November 16th 2008; the first transits of CoRoT-13b were discovered by the Alarm Mode and the target was oversampled (the standard 512s sampling rate was changed to 32s; see Surace et al. 2008) since December 9th 2008 and until the end of the observations in March 11th 2009, gathering in total about 250 000 photometric measurements.

The coordinates, identification labels and magnitudes of CoRoT-13 are given in Table 1. It is a relatively faint object for *CoRoT* ($V = 15.039$) and it was therefore assigned a monochromatic aperture mask (for a complete description of the observing modes of the satellite, please refer to Boisnard & Auvergne 2006; Barge et al. 2008; Auvergne et al. 2009). Figure 1 shows the raw light curve (LC) of the target. One of the most significant environmental effects in *CoRoT* LCs are hot pixels: proton impacts that produce permanent damage to the CCD lattice (see Drummond et al. 2008; Pinheiro da Silva et al. 2008). On average, 0.3% of the pixels are affected by one of these events with an impact of more than 1000 electrons in flux during a long run (Auvergne et al. 2009). The mask of CoRoT-13b has only 69 pixels, but unfortunately this particular LC shows at least 3 impacts over the 1000 electrons threshold plus some other impacts of less importance. These impacts do not affect significantly the characterization of the target as long as the regions affected are properly treated.

Canarias in the Spanish Observatorio del Teide. Part of the data presented herein were obtained at the W.M. Keck Observatory, which is operated as a scientific partnership among the California Institute of Technology, the University of California and the National Aeronautics and Space Administration. The Observatory was made possible by the generous financial support of the W.M. Keck Foundation.

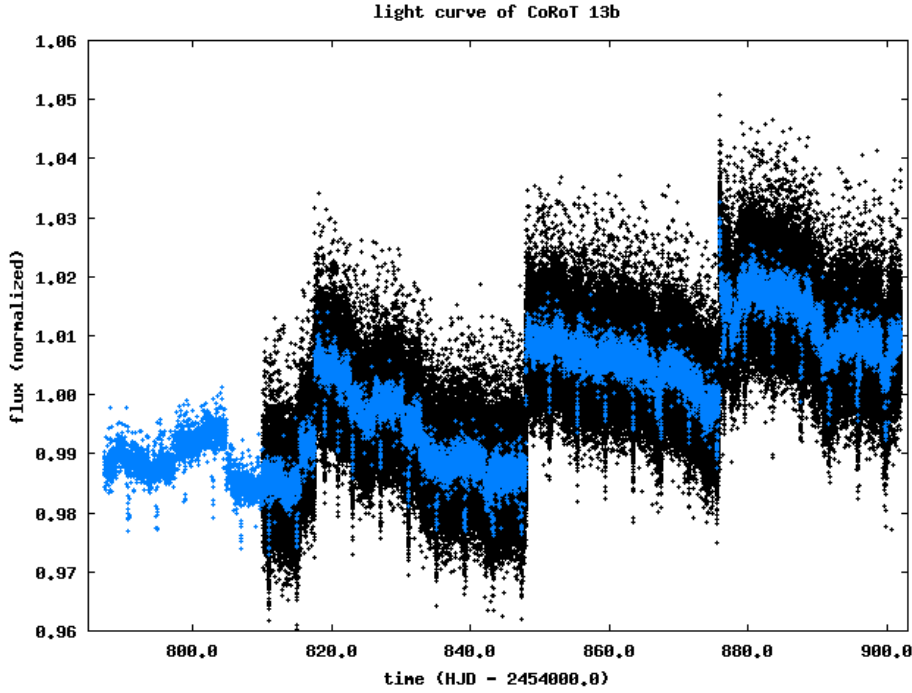


Fig. 1. Raw light curve of CoRoT-13b. The target was oversampled since December 9th 2008 (HJD 2454 810.20); for visualization purposes we superimpose the LC binned at a sampling rate of 512s to the 32s sampled region. The jumps in the data are from hot pixels as described in the text.

3. Ground-based observations

3.1. Photometric measurements

A complete description of the photometric follow-up of *CoRoT* targets is given in Deeg et al. (2009). For the particular case of CoRoT-13b, photometric measurements of the host star were carried out at the 3.6m Canada-France-Hawaii-Telescope (CFHT) in late November 2009 confirming that the transit was on-target, although with a depth slightly bigger than expected. This is due to the contribution of the contaminants to the flux in the *CoRoT* mask. Later on, in early January 2010, new on-off observations were carried out at the IAC80 telescope, in Tenerife, confirming the previous results.

Figure 2 shows the region of the sky around the target taken with the Wide Field Camera of the Isaac Newton Telescope (INT/WFC), in Roque de los Muchachos. The closest contaminants to the main target, according to the ExoDat database (Deleuil et al. 2009), are shown in Table 2. In particular, the object 110839426 is completely included in the *CoRoT* mask, diluting the transit signal of CoRoT-13b. An analysis of the point spread function (PSF) of *CoRoT* reveals that the main target, the planet-hosting star, is responsible for $89 \pm 1\%$ of the flux within the mask.

3.2. Spectroscopic measurements

The star was observed with HIRES at the Keck on Dec. 5th 2009 as part of the NASA’s key science programme in support of the *CoRoT* mission. Observations were made for 1200 sec without the iodine cell. The spectral resolution is $\sim 45\,000$. To determine the atmospheric parameters of CoRoT-13 we analyzed the spectrum using the VWA software (Bruntt et al. 2004, 2010a). We se-

Table 1. IDs, coordinates and magnitudes of CoRoT-13.

CoRoT window ID	LRa02_E2_2165	
CoRoT ID	110839339	
UCAC3	170-048045	
USNO-A2 ID	0825-03324928	
USNO-B1 ID	0849-0108714	
2MASS ID	06505307-0505112	
Coordinates		
RA (J2000)	6h 50m 53.07s	
Dec (J2000)	-5° 5' 11.26"	
Magnitudes		
Filter	Mag	Error
B ^a	15.777	0.077
V ^a	15.039	0.041
r ^a	14.738	0.027
i ^a	14.304	0.033
J ^b	13.710	0.021
H ^b	13.406	0.027
K ^b	13.376	0.038

Notes. ^(a) Provided by ExoDat Deleuil et al. (2009); ^(b) from 2MASS catalog.

Table 2. Closest contaminants to CoRoT-13b with their respective magnitudes and relative distances to the target.

CoRoT ID	distance (arc sec)	B	V	R
110839426	6.58	19.354	18.136	17.625
110839769	20.14	15.424	14.689	14.395
110838938	21.58	19.691	18.412	17.838
110838780	22.79	16.927	16.066	15.701
110838726	28.34	19.911	18.489	17.875
110839832	28.44	17.611	16.749	16.388

lected lines in the range 5050–7810 Å. A small section of the spectrum is shown in Fig. 3 where the typical signal-to-noise (SN) ratio is 55. To determine the atmospheric parameters we use the neutral and ionized Fe lines and also the wide Ca lines at 6122 and 6162 Å (see Bruntt et al. 2010a for a description). From this analysis we determine the parameters $T_{\text{eff}} = 5945 \pm 90$ K, $\log g = 4.30 \pm 0.10$, $[M/H] = +0.01 \pm 0.07$ (mean of Si, Fe and Ni), and projected rotational velocity $v \sin i = 4 \pm 1$ km/s. The T_{eff} has been adjusted by -40 K based on the comparison of 10 stars with T_{eff} determined from both interferometric and spectroscopic methods as described by Bruntt et al. (2010a). The abundances of 10 elements are given in Table 3 and shown in Fig. 4. The horizontal yellow bar is the mean metallicity. Although the metallicity of this star is essentially solar, it is notable that the

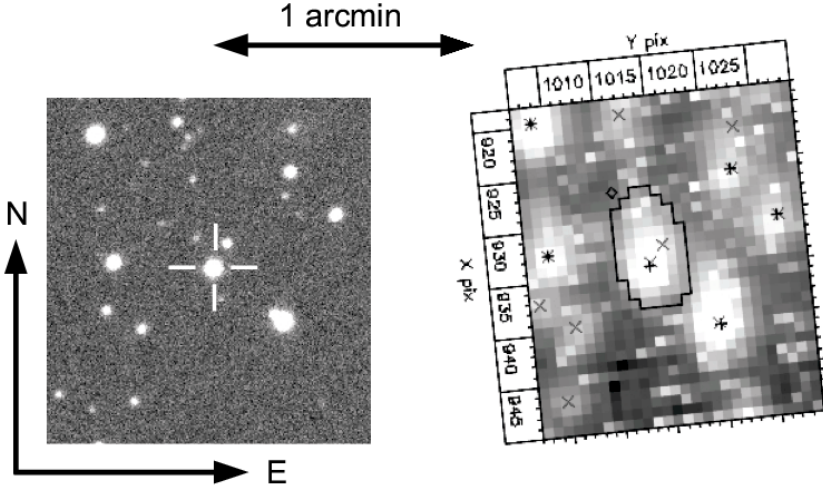


Fig. 2. Region of the sky around CoRoT-13. *Left:* Image taken with INT/WFC with a resolution of $0.3''$. The position of the target is indicated with a white cross. *Right:* Image taken by CoRoT with the same scale and orientation; the resolution is around $2.32''/\text{pixel}$. The area inside the black line is the mask used to compute the photometry; the position of the nearest contaminants from the ExoDat database are indicated with different types of crosses.

Table 3. Abundances of 10 elements in CoRoT-13 relative to the Sun. The element name, abundance relative to the Sun, and the number of spectral lines used are given.

El.	Abund.	N	El.	Abund.	N
Li I	+1.45	1	Ti I	-0.06	2
O I	+0.02	2	Ti II	+0.05 ± 0.04	2
Na I	-0.07	2	Cr I	-0.03 ± 0.16	4
Mg I	-0.07	1	Fe I	+0.03 ± 0.04	103
Si I	+0.04 ± 0.04	13	Fe II	+0.04 ± 0.05	11
Ca I	+0.03 ± 0.05	6	Ni I	-0.04 ± 0.05	25

abundance of Li I is +1.45 dex, in similarity to the case of another planet hosting star, CoRoT-6 (Fridlund et al. 2010).

Using Starevol tracks (Siess 2006) and the spectroscopic parameters, we derive the following stellar parameters: $M_* = 1.09 \pm 0.02 M_\odot$; $R_* = 1.01 \pm 0.03 R_\odot$; and a corresponding surface gravity of $\log g = 4.46 \pm 0.05$ which is in perfect agreement with the spectroscopic value. From the evolution tracks the corresponding age is between 0.12 and 3.15 Gyr.

Finally, using Allen (1973) to estimate the absolute V magnitude and the color excess (taking the $E_{J-K} = 0.0$ extinction into account), we calculate the distance to the star to be $d = 1\,310 \pm 100$ pc.

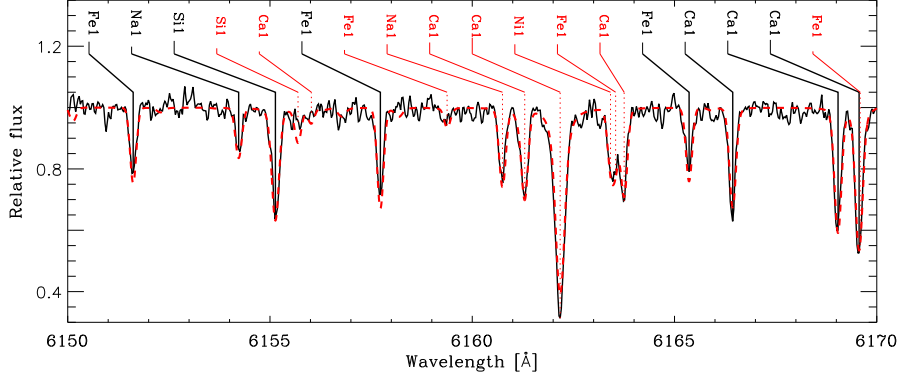


Fig. 3. Detail of the Keck spectrum of CoRoT-13 around the pressure-sensitive Ca II line at 6162 Å. The synthetic spectrum is shown with a dashed line. Spectral lines used in the abundance analysis are marked with solid vertical lines while the other spectral lines are marked with dotted lines.

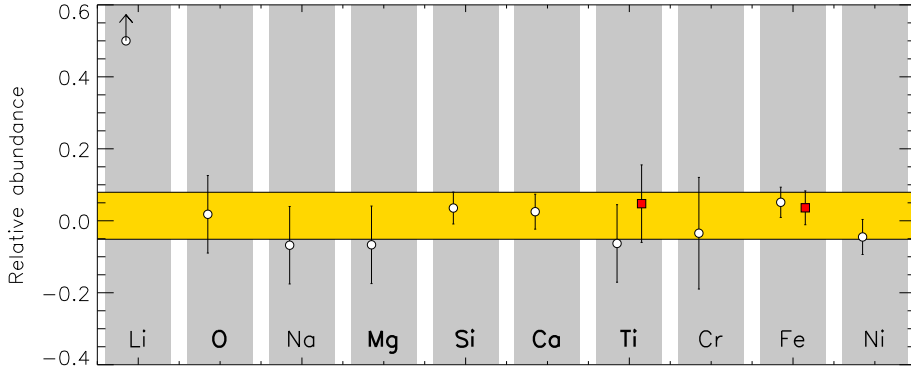


Fig. 4. Mean abundances for 10 elements in CoRoT-13 Keck spectrum. White circles correspond to neutral lines and red boxes stand for singly ionized lines. The yellow area represents the mean metallicity within one sigma error bar.

3.3. Radial Velocity measurements

Precise radial velocity measurements of CoRoT-13 were obtained with the HARPS spectrograph between the nights of November 22nd, 2009 and February 15th, 2010 (ESO program 184.C-0639). HARPS is a cross-dispersed echelle spectrograph fiber-fed from the Cassegrain focus of the 3.6 m telescope at La Silla Observatory, Chile (Mayor et al. 2003). Fifteen spectra with a spectral resolution $R \approx 115\,000$ were obtained using exposure times of 3600 s, and setting one of the two available fibers on the sky in order to monitor the presence of moonlight and to obtain an optimal sky background subtraction, which is important for faint targets such as this. The signal-to-noise ratios per pixel at 5500 Å of these observations range from 7.1 to 11.7. Th-Ar calibrations were obtained at the beginning of each night, which has been shown to be enough to obtain the required precision, due to the high stability of the instrument.

The spectra were reduced and extracted using the HARPS pipeline, and the radial velocity was measured on each extracted spectrum by means of a weighted cross-correlation (see Baranne et al. 1996) with a numerical mask corresponding to a G2 star. The resulting cross-correlation

functions (CCFs) were fit by Gaussians to get the radial velocities. The measured values are listed in Table 4 and shown in Fig. 5, together with the best fit orbital solution (see below). During some of the observations, the star fiber was contaminated by moonlight. In those cases, if the peak of the CCF produced by moonlight was expected to be close to the measured speed of the target, a correction was applied using the fiber which recorded the sky (see Bonomo et al. 2010, in preparation). Those points are shown as white circles in Fig. 5 and we added quadratically 30 m s^{-1} to the uncertainty estimated from the CCF, in order to account for possible systematic errors introduced by the moonlight correction.

The orbital solution was found by χ^2 minimization, with the period and epoch of inferior conjunction (when radial velocity is zero after removal of the systemic velocity) being fixed to the values provided by the *CoRoT* ephemeris. The eccentricity of the orbit was a free parameter at first, but since the best fit solution was compatible with a circular orbit at the two- σ level (the three- σ upper limit to the eccentricity is 0.145), we decided to fix it to $e = 0$ for the determination of the rest of the parameters and their uncertainties. Figure 5 shows the RV measurements, phased to the *CoRoT* period, together with the best fit circular model and the residuals; the obtained parameters are listed in Table 6. The resulting value of χ^2 is 8.2 for 13 degrees of freedom, and the *rms* of the residuals is 20.2 m s^{-1} , which is compatible with what should be expected based on the median of the RV uncertainties, 21.2 m s^{-1} . These facts suggest that the circular model – with the obtained parameters – adequately describes the available data.

With fixed ephemeris and eccentricity set to zero, the fitting problem is reduced to a linear least-square minimization with two free parameters. The uncertainties reported in Table 6 are therefore estimated by means of the covariance matrix, which has a covariance term of $6.48 \text{ m}^2 \text{ s}^{-2}$. However, stellar activity and other long-term phenomena can produce correlated noise in the observations and hence render the above estimation of the uncertainties invalid. In order to explore this we used the Prayer Bead method (see, for example, Désert et al. 2009; Winn et al. 2009), i.e. we performed a cyclic permutation of the residuals of the best fit curve and fit the model again. We repeated this for every possible shift and measured the standard deviation of the obtained parameters. We also performed a similar analysis but randomly re-ordering the residuals rather than shifting them. In this way, we constructed 10000 synthetic data sets that were used to fit our model again. In both cases, the obtained dispersion of the parameters were smaller than the error bars reported in Table 6.

The bisector analysis for these data is shown in Fig 6, where the uncertainty in the bisector span velocity has been set to twice that of the corresponding radial velocity. The bisector span velocities do not show any clear dependence with radial velocity values and the Pearson correlation coefficient between these two magnitudes is around 0.15, which is a sign of lack of correlation. This fact clearly indicates that the measured RV variations do not originate from changes in the shape in the CCF as would be the case if the system consisted of a background eclipsing binary whose light were diluted by the *CoRoT* main target. Additionally, no significant changes in the measured RV are observed when different stellar masks are used for the correlation, which further excludes the background eclipsing binary scenario.

Table 4. Radial velocities measurements and bisector span velocities measured with HARPS.

BJD	RV	σ_{RV}	Bis	Moon Correction ^a
-2455000	[km/s]	[km/s]	[km/s]	[km/s]
158.7187	22.293	0.029	0.027	
160.725	22.598	0.026	0.038	
161.7209	22.522	0.053	0.144	0.101
163.8279	22.379	0.044	-0.019	0.055
166.7245	22.311	0.037	-0.091	0.219
168.7634	22.641	0.042	-0.012	0.503
219.7315	22.296	0.02	0.036	
220.7327	22.464	0.022	-0.014	
225.6511	22.606	0.021	-0.01	
226.7338	22.45	0.021	0.059	
228.6545	22.452	0.021	-0	
237.5841	22.624	0.02	0.006	
238.5617	22.478	0.018	-0.014	
239.7142	22.304	0.019	0.024	
243.6139	22.311	0.016	-0.003	

^(a) Difference between moonlight-corrected and uncorrected radial velocities.

4. Planetary parameters

The transit parameters were determined in the same manner as described in the case of CoRoT-6b (Fridlund et al. 2010). The pre-processed light curve was divided by its median, and a new light curve was constructed by convolving it with a fourth order Savitzky-Golay filter (Press et al. 2002). The standard deviation of the differences between the measured and the convolved light curves is calculated and a 5σ clip is applied to remove spurious outliers. This clipping is iterated until no more outliers are found. After these steps, the light curve is folded and a bin average is applied forming 5000 bins.

We used the Mandel & Agol (2002) model to perform the fit to the final, phase-folded light curve. We assumed a circular orbit and an absolutely dark planet at the CoRoT wavelength. Our six adjusted parameters were: the a/R_s , $k = R_{pl}/R_s$ ratios, the impact parameter $b = a \cos i/R_s$ (i is the inclination of the orbit) and the two limb darkening coefficients u_+ , u_- (a quadratic limb darkening law was used). The sixth parameter was the contaminant factor which was varied between 10-12% (corresponding to the measured value of $11 \pm 1\%$) to allow a better estimation of errors. The best fit was found by the Harmony Search algorithm (Geem et al. 2001), a genetic-type algorithm. The 1σ errors were obtained from the width of the parameter distribution to be between χ_{\min}^2 and $\chi_{\min}^2 + 1$.

We calculated different solutions for the light curve of CoRoT-13b using different approaches in the treatment of the limb darkening parameters in order to understand the constraints that this effect puts in the determination of the final values. The results are presented in Table 5. In model A we left both u_+ and u_- to be free parameters. In models B, C and D we fixed u_+ at 0.81 (the value what we found in model A), at 0.88 (i.e. $0.81 + 1\sigma$) and 0.74 ($0.81 - 1\sigma$; where σ means the error bar of the coefficient found in model A) respectively. In model E we fixed the limb darkening to the predicted values for the star (Sing 2010). The corresponding χ^2 -values of these solutions

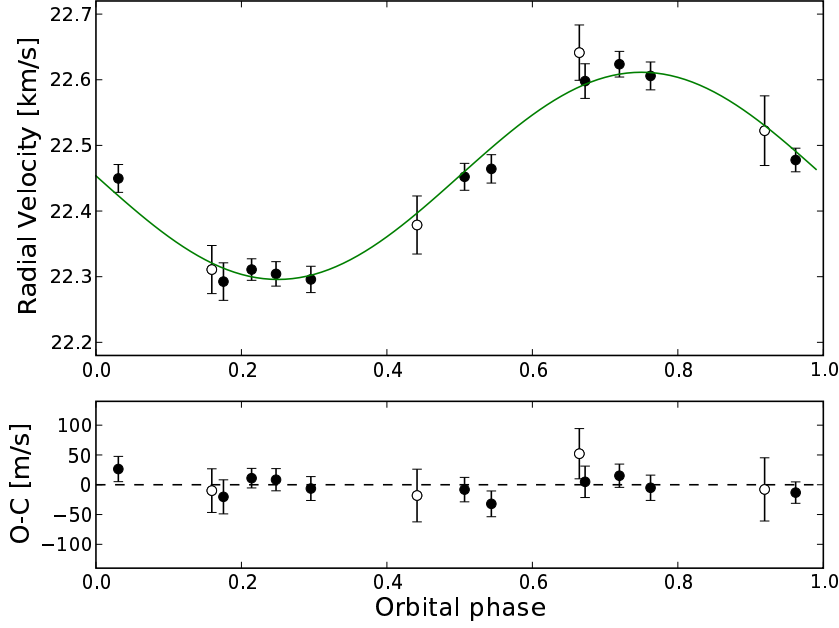


Fig. 5. *Upper panel:* Radial Velocity measurements phased to the orbital period measured by *CoRoT*. The solid curve represents the best fit solution. *Lower panel:* Residuals to the fit. In both panels, the white symbols indicate the measurements that have been corrected for moonlight contamination.

were not too different from each other, showing that limb darkening is a second order effect in the transit shape. The different assumptions for the limb-darkening yielded quite consistent light curve solutions: the a/R_s , k ratios are in good agreement well within their error bars in these five models. When we fixed u_+ , the uncertainties of the impact parameter increased by a factor of two, however, the error bars of impact parameters found in the B, C, D and E solutions are overlapping with the one found in model A. The precise determination of the impact parameter is more complicated when the transit is nearly central. We learn from this experiment that fitting both limb darkening coefficients (or, what we actually did, fitting both of their combinations) yielded a bit more precise values.

Since $u_+ = 0.81 \pm 0.07$ (Sing 2010 gives 0.662 ± 0.022 for this temperature, $\log g$ and metallicity) and $u_- = -0.09 \pm 0.09$ (Sing 2010 gives 0.156 ± 0.022) the agreement between theoretical predictions and measurements is within 2 sigma error bars. This seems to be quite satisfactory at this stage of the theory. Interestingly, solution D is closer to the theoretical predictions, but there are no further indications that this better agreement constitutes also a more correct description of the system. We accept solution A as the definitive one (the fit is shown in Fig. 7).

5. Discussion

5.1. Stellar properties

The spectroscopic analysis of CoRoT-13 reveals a G0V star with an age between 0.12 and 3.15 Gyr, solar metallicity ($[M/H] = +0.01 \pm 0.07$), a high relative abundance of lithium (+1.45 dex), and a low activity level according to the analysis of activity indicators such as the H-K Ca II lines.

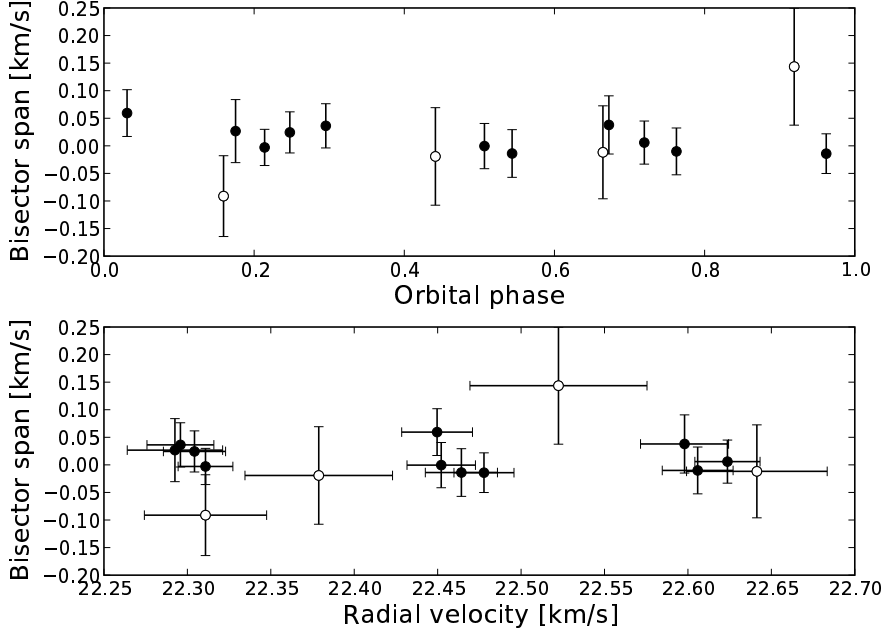


Fig. 6. Bisector analysis of the HARPS data. The white symbols represent measurements that have been corrected for moonlight contamination.

Table 5. Values of the adjusted parameters in the modeling of the transit of CoRoT-13b in the different approximations described in the text.

Parameter	A	B	C	D	E
a/R_*	10.81 ± 0.32	11.22 ± 0.42	11.15 ± 0.40	10.98 ± 0.48	10.89 ± 0.40
$k = R_p/R_*$	0.0909 ± 0.0014	0.0900 ± 0.0016	0.0896 ± 0.0014	0.0912 ± 0.0012	0.0914 ± 0.0011
$b = a \cos i/R_*$	0.374 ± 0.054	0.264 ± 0.097	0.271 ± 0.092	0.349 ± 0.091	0.385 ± 0.070
inclination (deg)	$88.01^{+0.35}_{-0.33}$	$88.65^{+0.57}_{-0.53}$	$88.61^{+0.54}_{-0.50}$	$88.01^{+0.58}_{-0.53}$	$87.97^{+0.43}_{-0.46}$
u_+	0.81 ± 0.07	0.81 (fixed)	0.88 (fixed)	0.74 (fixed)	0.662 (fixed)
u_-	-0.09 ± 0.09	-0.09 (fixed)	-0.24 ± 0.32	-0.01 ± 0.25	0.156 (fixed)
third light	0.11 ± 0.01	0.11 ± 0.01	0.11 ± 0.01	0.11 ± 0.01	0.11 ± 0.01
$\chi^2(a)$	1.00000	1.00039	0.99945	1.00077	1.00130

Notes. ^(a) Normalized to the value of solution A

The rate of lithium depletion of solar like stars is related to the age of the star and to the depth of the convective zone, as it is destroyed at a temperature of approximately $\sim 2.5 \cdot 10^6$ K in the radiative region of a star (Chaboyer 1998). Given the spectral type of CoRoT-13, we expect a lower lithium depletion rate than in solar analogs (Castro et al. 2009). Using the value of the Li I abundance, we compute a $\log n(Li) = 2.55$. From Fig. 7 of Sestito & Randich 2005 and with the value of the effective temperature ($T_{\text{eff}} = 5945 \pm 90$ K) we estimate the age of the star in the range 300 Myr to 1 Gyr, consistent with the range from the evolutionary models. In a recent paper, Israelian et al. (2009) claim a lithium depletion in solar like stars with orbiting planets, although it is not clear that previous observations support this conclusion (Meléndez et al. 2009b). CoRoT-13 is not depleted

Table 6. Planet and star parameters.

<i>Ephemeris</i>	
Planet orbital period P [days]	$4.035\,190 \pm 0.000\,030$
Primary transit epoch T_{tr} [HJD-2 450 000]	$4\,790.809\,1 \pm 0.000\,6$
Primary transit duration d_{tr} [h]	3.14 ± 0.01
<i>Results from radial velocity observations</i>	
Orbital eccentricity e	0 (fixed)
Radial velocity semi-amplitude K [m s^{-1}]	157.8 ± 7.7
Systemic velocity V_r [km s^{-1}]	22.4536 ± 0.0060
O-C residuals [m s^{-1}]	20.2
<i>Fitted transit parameters</i>	
Radius ratio $k = R_p/R_*$	$0.090\,9 \pm 0.001\,4$
Linear limb darkening coefficients ^a u_+	0.81 ± 0.07
u_-	-0.09 ± 0.09
Impact parameter ^b b	0.374 ± 0.054
<i>Deduced transit parameters</i>	
Scaled semi-major axis a/R_*	10.81 ± 0.32
$M_*^{1/3}/R_*$ [solar units]	1.014 ± 0.030
Stellar density ρ_* [g cm^{-3}]	1.468 ± 0.131
Inclination i [deg]	$88.02^{+0.34}_{-0.36}$
<i>Spectroscopic parameters</i>	
Effective temperature T_{eff} [K]	$5\,945 \pm 90$
Surface gravity $\log g$ [dex]	4.30 ± 0.10
Metallicity [Fe/H] [dex]	0.01 ± 0.07
Stellar rotational velocity $v \sin i$ [km s^{-1}]	4 ± 1
Spectral type	G0V
<i>Stellar and planetary physical parameters from combined analysis</i>	
Star mass [M_\odot]	1.09 ± 0.02
Star radius [R_\odot]	1.01 ± 0.03
Distance of the system [pc]	$1\,310 \pm 100$
Stellar rotation period P_{rot} [days]	13^{+5}_{-3}
Age of the star t [Gyr]	$0.12 - 3.15$
Orbital semi-major axis a [AU]	0.0510 ± 0.0031
Planet mass M_p [M_{Jup}] ^d	1.308 ± 0.066
Planet radius R_p [R_{Jup}] ^d	0.885 ± 0.014
Planet density ρ_p [g cm^{-3}]	2.34 ± 0.23
Average surface temperature ^e T_p [K]	$\sim 1\,700$

Notes. ^(a) $I(\mu)/I(1) = 1 - u(1 - \mu)$, where $I(1)$ is the specific intensity at the center of the disk and $\mu = \cos \gamma$, γ being the angle between the surface normal and the line of sight; ^(b) $b = \frac{a \cos i}{R_*}$ ^(d) Radius and mass of Jupiter taken as 71492 km and $1.8986 \times 10^{30} \text{ g}$, respectively. ^(e) Zero albedo equilibrium temperature for an isotropic planetary emission.

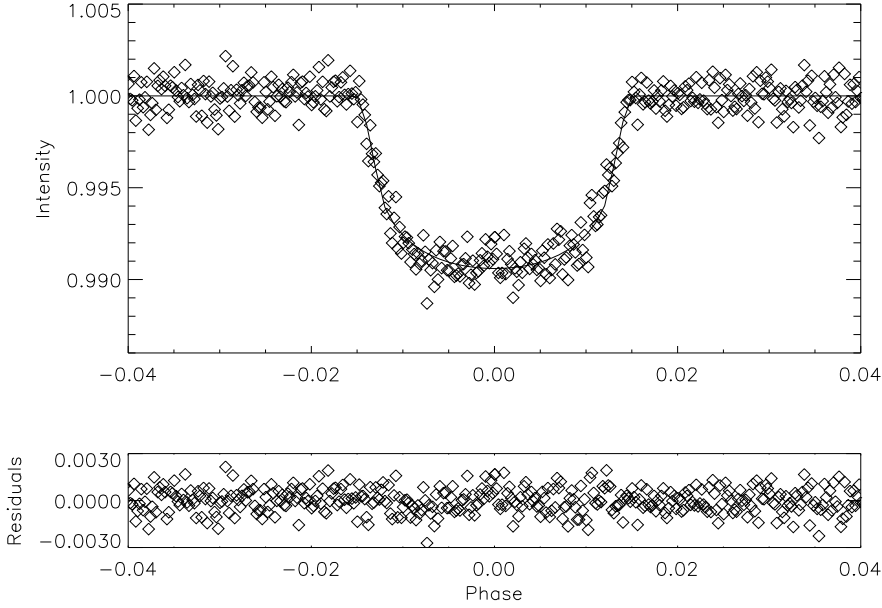


Fig. 7. Folded transit of CoRoT-13b, best fit and its residuals using the values of solution A in Table 5.

in lithium, albeit we call the attention to the fact that the effective temperature of this star is slightly higher than the upper limit for depletion given in Israelian et al. (2009).

The $\nu \sin i$ value indicates a rotational period of the star of around 13 days¹. According to this value, a $(B - V)_0 = 0.60$; gyro-chronologically predicts an age of 1.4 Gyr (Barnes 2007) which is in agreement within the range of age given by evolutionary models. The latter paper recalls an equation that links the age and the activity level and the expected value of $\log R'_{HK}$ is ~ -6.0 ; which is very low and consistent with our observations. Other G0V stars are found with similar rotation rates and low activity levels (Noyes et al. 1984).

We have looked for signs of stellar rotation in the light curve (LC) observed by *CoRoT* to make a comparison with the clear signs of spot modulation found in the cases of CoRoT-2b (Lanza et al. 2009b), CoRoT-4b (Lanza et al. 2009a), CoRoT-6b (Fridlund et al. 2010) or CoRoT-7b (Lanza et al. 2010). The Lomb-Scargle periodogram of the LC, once the planetary transits have been removed and the hot-pixel events have been treated, shows indeed a significant broad peak around 77 days; but not any significant peak at the expected rotational frequencies. The 77 days period is comparable with the length of the run (115 days), so it might be that we are observing an irregular pattern that, in the observing window of 115 days, has a typical timescale of variation of 77 days that may mimic an harmonic oscillation. The only reliable information on the nature of this particular signal is its characteristic amplitude of 0.5% and its characteristic timescale of 77 days; one has to be extremely cautious when interpreting its nature. Two immediate possibilities are stellar activity and an instrumental residual signal. In the latter case, stray light or other instrumental effects such as temperature fluctuations should affect a region of the CCD (if not all), instead of a single target. None of the targets in the neighborhood of CoRoT-13 show a similar pattern. Other environmental features (such as hot pixels) although present, have a completely different behavior both

¹ a lower limit, as the value of $\sin i$ for the spin axis of the star is unknown.

in amplitude and in timescale and are not likely to be responsible for the signal. The spectroscopic analysis shows that CoRoT-13 is a quiet dwarf star. A G0V star might show spot modulation with a characteristic timescale similar to the rotational period of the star as well as long term variations in timescales of several years (Baliunas et al. 1995), but not in the timescales considered here. On the other hand, slow rotating giant stars might show a pattern of variability with similar amplitudes and characteristic timescales as the ones revealed by the periodogram. We therefore conclude that the modulation measured in the LC of *CoRoT* is due to a background contaminant and not to the main target.

In a recent paper, Lanza (2010) links the presence of giant planets and the angular momentum loss of their host stars, detecting that giant planet hosting stars with $T_{\text{eff}} \gtrsim 6000\text{K}$ tend to be in a $n/\Omega \approx 1, 2$ orbital period/rotational period synchronization with their respective planets. The effective temperature of CoRoT-13 lays right below this lower limit and indeed the rotational period obtained from the spectroscopic analysis (around 13 days) is longer than the expected 2:1 resonance or the synchronization; although the rotational period is not sufficiently well constrained (the relative uncertainty is around 35%) and the inclination of the spin-axis of the star is not known. A study of the Rossiter-McLaughlin effect of this planet will provide the relative angle of inclination of the planet and the star, which is an important parameter in the model proposed by Lanza (2010).

5.2. Planet interior

Figure 8 compares CoRoT-13b to other transiting exoplanets in a mass-radius diagram. Although it is not the densest object known so far (both super-Earths and brown dwarfs may be denser), it is clearly extremely dense for its mass. This is confirmed by a combined modeling of the star and planet evolution (see Bordé et al. 2010; Morel & Lebreton 2008; Guillot & Morel 1995) shown in Fig. 9. The small planetary radius derived from the transit photometry and spectroscopy can be explained only by advocating the presence of a truly considerable amount of heavy elements in the planet. When fitting the stellar effective temperature and density within their 1-sigma error bars (see Table 6 and red area in Fig. 9), between about 140 and 300 M_{\oplus} of heavy elements are required to reproduce the measured planetary size. When fitting the stellar parameters only within 3σ (yellow area), still at least 100 M_{\oplus} of heavy elements are needed. In our planetary evolutions calculations, we assumed all heavy elements to be grouped into a well-defined central core, surrounded by a solar-composition envelope, with no added sources of heat. The possibility that these heavy elements may be at least partly mixed in the envelope is not expected to change these numbers significantly (Guillot 2005; Ikoma et al. 2006; Baraffe et al. 2008).

This extremely high amount of heavy elements is surprising for several reasons: first, this is probably a record - HD149026b, a Saturn-mass planet, has been known to possess about 60–70 M_{\oplus} of heavy elements (Sato et al. 2005; Ikoma et al. 2006). Other objects, such as OGLE-TR-56b and OGLE-TR-132b were also later shown to have close to 100 M_{\oplus} in heavy elements (Guillot et al. 2006), but no planetary-mass object was yet shown to possess more heavy elements. An exception may be HAT-P-2b, initially thought to have $M_Z = 200$ to 600 M_{\oplus} (Baraffe et al. 2008; Leconte et al. 2009), but a revision of the stellar parameters (Torres et al. 2008) yields much smaller M_Z values for this object.

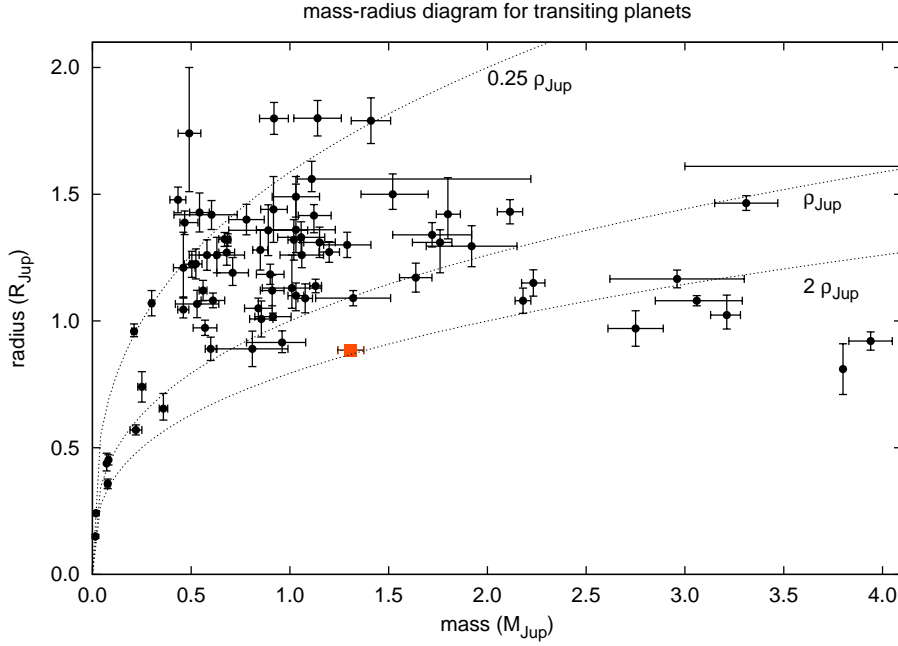


Fig. 8. Position of CoRoT-13b (square) among the other transiting planets in a mass-radius diagram.

Second, planet formation models do not predict the existence of such dense objects (Mordasini et al. 2009). This is because a protoplanetary core growing beyond a few tens of Earth masses rapidly captures any surrounding hydrogen and helium, and that the accretion of planetesimals is suppressed by the growth of the protoplanet beyond Saturn’s mass. Giant impacts need to be invoked for a further capture of a significant mass of heavy elements (Ikoma et al. 2006).

Third, CoRoT-13b is a counterexample outside the correlation between stellar-metallicity and planetary mass in heavy elements (Guillot et al. 2006; Burrows et al. 2007; Guillot 2008). One interesting possibility however is related to the high lithium abundance of the star. If the metallicity of stars with planets in fact tell us about the late accretion of circumstellar gas filtered of their heavy elements by planet formation (Meléndez et al. 2009b; Ramírez et al. 2009; Nordlund 2009), it raises the possibility that the CoRoT-13 system was in fact metal-rich, but that a heavy-elements poor, lithium-rich rare last burst of accretion modified the chemical properties of the star’s thin outer convective zone.

5.3. Thermal losses

We estimate the thermal mass loss of CoRoT-13b by using the method and formulae described in Lammer et al. (2009), and we find a negligible escape rate which did not influence the planets mass over its history. The reason of the negligible thermal mass loss of CoRoT-13b is the planets compactness and high density of about 2.34 g cm^{-3} .

5.4. Occultation of the planet by the star

In the visible wavelength range, occultations of planets behind their host stars have to date been detected only in a few cases: Corot-1b (Snellen et al. 2009; Alonso et al. 2009a) and CoRoT-2b (Alonso et al. 2009b; Snellen et al. 2010) in data from *CoRoT* and HAT-P-7 in data from Kepler

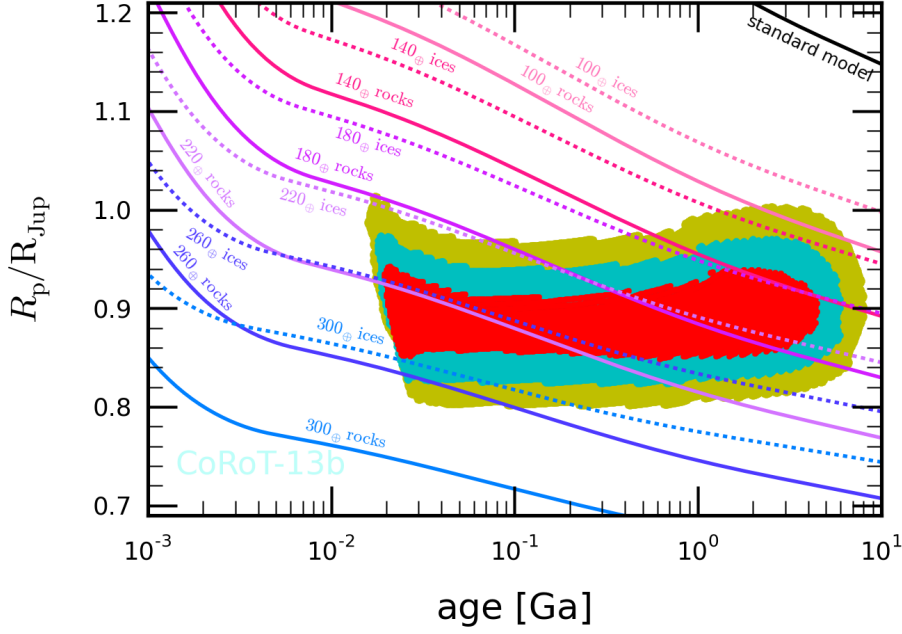


Fig. 9. Age (in Ga= 10^9 years) versus transit radius of CoRoT-13b (in Jupiter units, $1R_{\text{Jup}}=71\,492$ km). The colored area correspond to constraints derived from stellar evolution models matching the stellar density and effective temperature within a certain number of standard deviations: less than 1σ (red), 2σ (blue) or 3σ (yellow). The curves are evolution tracks for CoRoT-13b (assuming $M = 1.308M_{\text{Jup}}$, $T_{\text{eq}} = 1700$ K), with various models as labelled

(Borucki et al. 2009). All are inflated giant planets ($R_p > 1.4R_{\text{Jup}}$) on very short orbits, which means that they have large surfaces favoring a large flux of reflected light and additionally they are very hot ($T_{\text{eff}} > 2000$ K), which favors thermal emission in the visible regime. Using the definition from Cowan & Agol (2010), CoRoT-13b, in the most favorable case (zero albedo, zero heat redistribution factor; upper solid line in Fig. 10), should have an average surface temperature around 1700 K. The emission of the planet in the visible range observed by *CoRoT* is therefore dominated by reflection, meaning that eclipse amplitudes larger than $2.5 \cdot 10^{-5}$ cannot be expected, even with a very high Bond albedo of $A_B = 0.5$ (Fig. 10, dotted lines). Such a signal is however not detectable in the current data, as the measured scatter in the folded and binned light curve is on the order of 10^{-4} .

5.5. Constraints on the presence of additional planets.

The region of the light curve (LC) shown in Fig. 11, between the 8th and the 9th transits observed by *CoRoT* shows a feature which mimics a single planetary transit not related to the pattern of transits of CoRoT-13b. Almost in the middle point of the two regular transits we find a short feature, roughly 1.5h long and 1% deep which in principle could be due to a planetary transit from an additional planet in the system. This feature does not repeat in the LC so that a hypothetical companion would need a period longer than the 80 days that remained until either end of the observations. Nevertheless, the duration of a planetary transit is linked to the period of the orbit (Seager & Mallén-Ornelas 2003) and for an 80 days orbit we expect a transit around 8 hours long.

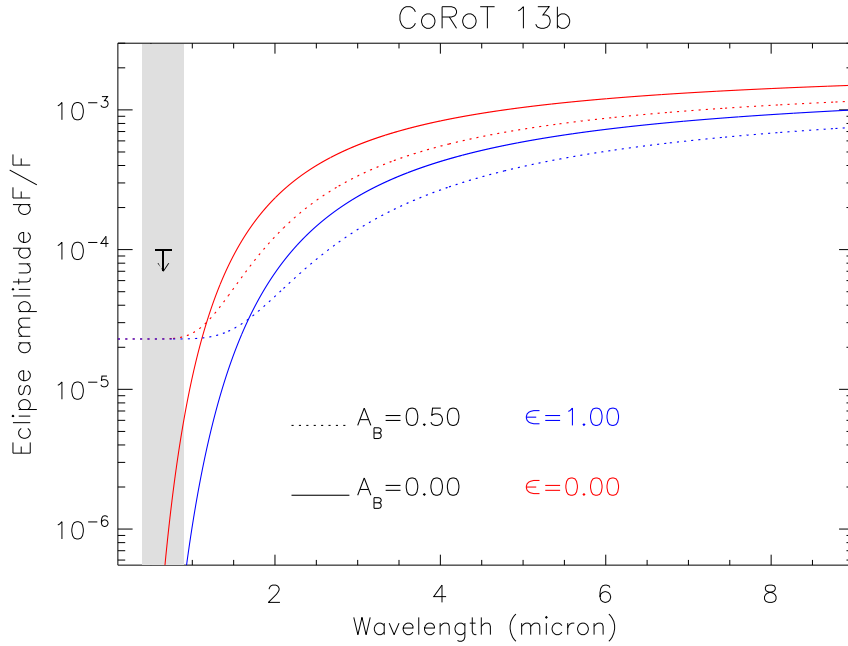


Fig. 10. Expected amplitude of the occultation of the planet as a function of the wavelength for two extreme values for the heat redistribution factor for CoRoT-13b (as defined by Cowan & Agol 2010; $\epsilon = 1$: uniform heat distribution over the planet; $\epsilon = 0$ no distribution) and two values of the Bond albedo. The gray shaded area is the wavelength window observed by *CoRoT*. The black arrow is the upper limit of *CoRoT* observations.

Of course, some corrections have to be done in the case the orbit is eccentric (Carter et al. 2008; Kipping 2008); but in our case we would have to admit an eccentricity of 0.94 (and a favorable orientation) for the hypothetical planet to have a 1.5h long transit in such a long period orbit. However, this hypothetical planet would have a periastron passage inside the orbit of CoRoT-13b. There are studies of the planetary three body problem with high eccentricities (see for example Beaugé & Michtchenko 2003; Michtchenko et al. 2006), but to the knowledge of the authors there is no possible justification for the dynamical stability of one system formed by a close-in Jupiter-like planet in a circular orbit and a highly eccentric Jupiter-sized companion.

Moreover, there is no hint of the drift produced by any additional planet in the scatter of the residuals of the circular radial velocity (RV) analysis. The region of the parameter space of an additional planet in a circular orbit which can be discarded based on RV data is shown in Fig 12. We note that for periods below 85 days (the span of HARPS observations), only planets in circular orbits with masses below $\sim 0.45 M_{\text{Jup}}$ are not discarded by RV data. The mass limit for eccentric orbits is even lower in this range of periods, as the amplitude K of the RV movement grows as $(1 - e^2)^{-1/2}$.

Given these facts, the most simple explanation is an environmental effect that mimics a transit.

6. Summary

We have reported the discovery of CoRoT-13b, a transiting giant planet orbiting the star *CoRoT* 110839339.

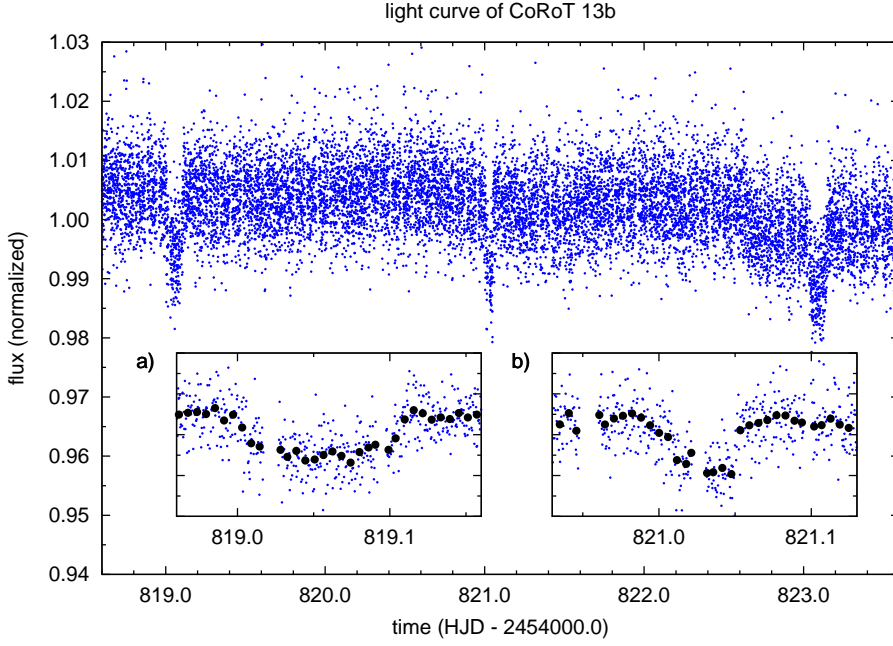


Fig. 11. Raw light curve of CoRoT-13b between the observed transits number 8 (HJD=2 454 819.06) and 9 (HJD=2 454 823.09). a) is a detail of the 8th transit. b) is a detail of the event at HJD=2 454 821.03 which mimics the transit of a long period planetary companion.

The spectroscopic analysis reveals that CoRoT-13 is a G0V star with $T_{\text{eff}} = 5\,945\text{K}$, $M_* = 1.09M_{\odot}$, $R_* = 1.01 \pm 0.03R_{\odot}$, solar metallicity ($[M/H] = +0.01 \pm 0.07$) and a high relative abundance of lithium (+1.45 dex). The evolutionary tracks constrain the age of the star between 0.12 and 3.15 Gyr. The results of the study of the lithium abundance, the $v \sin i$ and the activity level (which is low both in the spectroscopic and in the photometric analysis) are consistent with the spectral type and the age range of the star; although the lower limit of the interval is not favored due to the low activity level measured.

CoRoT-13b is the highest density jovian planet among its relatives with masses between 0.2 and 2.5 Jupiter masses. Its extreme density implies the existence of a significant amount, between 140 and $300M_{\oplus}$, of heavy elements in the planet, which is contradiction with the expected link between M_Z of a planet and the metallicity of its host stars (Guillot et al. 2006; Burrows et al. 2007; Guillot 2008).

There is no hint of any other massive companion in the system, which is quite a common case for hot Jupiters.

We have discussed the consequences of this characterization and we show evidence that this particular target provides important information for the knowledge of the interactions between the structure of stars, the formation of planets, and their joint evolution (Ikoma et al. 2006; Ammler-von Eiff et al. 2009; Meléndez et al. 2009a; Nordlund 2009; Ramírez et al. 2009; Lanza 2010).

Transit surveys are biased towards planets with large radii and hence lower densities. We might be unveiling the high-density part of the planet distribution with *CoRoT* high-quality light curves.

Acknowledgements. The team at IAC acknowledges support by grant ESP2007-65480-C02-02 of the Spanish Ministerio de Ciencia e Innovación. This research has made use of the ExoDat database, operated at LAM-OAMP, Marseille, France, on behalf of the CoRoT/Exoplanet program. This publication makes use of data products from the Two Micron All Sky Survey,

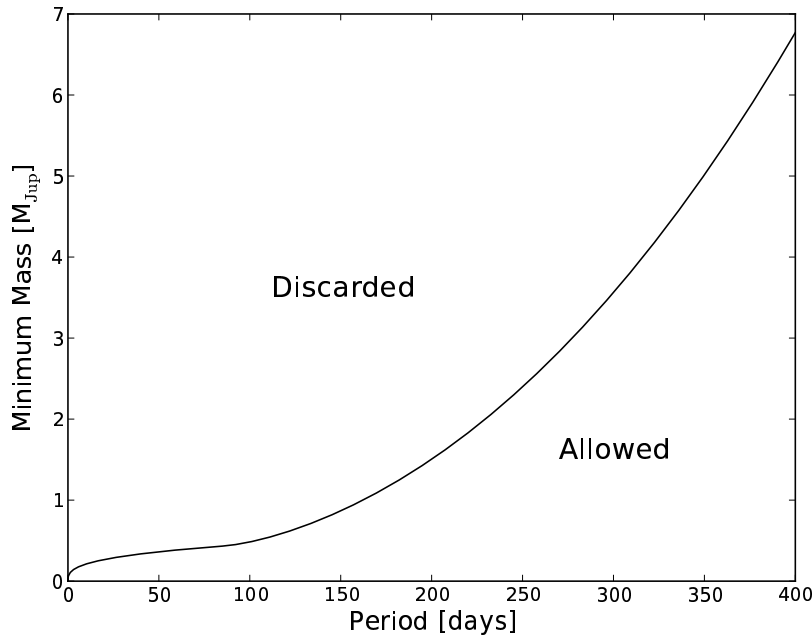


Fig. 12. Parameter space of the additional planets in the system which can be discarded with current HARPS measurements. The region above the curve is discarded by RV measurements, while planets located in the region below the curve would produce an undetectable signal.

which is a joint project of the University of Massachusetts and the Infrared Processing and Analysis Center/California Institute of Technology, funded by the National Aeronautics and Space Administration and the National Science Foundation. This research has made use of NASA's Astrophysics Data System.

References

- Allen, C. W. 1973, *Astrophysical quantities* (London: University of London, Athlone Press, —c1973, 3rd ed.)
- Alonso, R., Alapini, A., Aigrain, S., et al. 2009a, *A&A*, 506, 353
- Alonso, R., Guillot, T., Mazeh, T., et al. 2009b, *A&A*, 501, L23
- Ammler-von Eiff, M., Santos, N. C., Sousa, S. G., et al. 2009, *A&A*, 507, 523
- Auvergne, M., Bodin, P., Boissard, L., et al. 2009, *ArXiv e-prints*
- Baglin, A., Auvergne, M., Boissard, L., et al. 2006, in *COSPAR, Plenary Meeting, Vol. 36, 36th COSPAR Scientific Assembly*, 3749
- Baliunas, S. L., Donahue, R. A., Soon, W. H., et al. 1995, *ApJ*, 438, 269
- Baraffe, I., Chabrier, G., & Barman, T. 2008, *A&A*, 482, 315
- Baranne, A., Queloz, D., Mayor, M., et al. 1996, *A&AS*, 119, 373
- Barge, P., Baglin, A., Auvergne, M., & the CoRoT team. 2008, in *IAU Symposium, Vol. 249, IAU Symposium*, 3–16
- Barnes, S. A. 2007, *ApJ*, 669, 1167
- Beaugé, C. & Michtchenko, T. A. 2003, *MNRAS*, 341, 760
- Boissard, L. & Auvergne, M. 2006, in *ESA Special Publication, Vol. 1306, ESA Special Publication*, ed. M. Fridlund, A. Baglin, J. Lochard, & L. Conroy, 19
- Bordé, P., Bouchy, F., Deleuil, M., et al. 2010, *A&A*
- Borucki, W. J., Koch, D., Jenkins, J., et al. 2009, *Science*, 325, 709
- Bruntt, H., Bedding, T. R., Quirion, P., et al. 2010a, *ArXiv e-prints*
- Bruntt, H., Bikmaev, I. F., Catala, C., et al. 2004, *A&A*, 425, 683
- Bruntt, H., Deleuil, M., Fridlund, M., et al. 2010b, *ArXiv e-prints*

- Burrows, A., Hubeny, I., Budaj, J., & Hubbard, W. B. 2007, *ApJ*, 661, 502
- Carter, J. A., Yee, J. C., Eastman, J., Gaudi, B. S., & Winn, J. N. 2008, *ApJ*, 689, 499
- Castro, M., Vauclair, S., Richard, O., & Santos, N. C. 2009, *A&A*, 494, 663
- Chaboyer, B. 1998, in *IAU Symposium, Vol. 185, New Eyes to See Inside the Sun and Stars*, ed. F.-L. Deubner, J. Christensen-Dalsgaard, & D. Kurtz, 25–+
- Cowan, N. B. & Agol, E. 2010, *ArXiv e-prints*
- Deeg, H. J., Gillon, M., Shporer, A., et al. 2009, *A&A*, 506, 343
- Deeg, H. J., Moutou, C., Erikson, A., et al. 2010, *Nature*, 464, 384
- Deleuil, M., Meunier, J. C., Moutou, C., et al. 2009, *AJ*, 138, 649
- Désert, J., Lecavelier des Etangs, A., Hébrard, G., et al. 2009, *ApJ*, 699, 478
- Drummond, R., Lapeyrere, V., Auvergne, M., et al. 2008, *A&A*, 487, 1209
- Fridlund, M., Hébrard, G., Alonso, R., et al. 2010, *A&A*, 512, A14
- Geem, Z. G., Kim, J. H., & Loganathan, G. V. 2001, *Simulation*, 76, 60, <http://sim.sagepub.com/cgi/content/abstract/76/2/60>
- Guillot, T. 2005, *Annual Review of Earth and Planetary Sciences*, 33, 493
- Guillot, T. 2008, *Physica Scripta Volume T*, 130, 014023
- Guillot, T. & Morel, P. 1995, *A&AS*, 109, 109
- Guillot, T., Santos, N. C., Pont, F., et al. 2006, *A&A*, 453, L21
- Ikoma, M., Guillot, T., Genda, H., Tanigawa, T., & Ida, S. 2006, *ApJ*, 650, 1150
- Israeliian, G., Delgado Mena, E., Santos, N. C., et al. 2009, *Nature*, 462, 189
- Kipping, D. M. 2008, *MNRAS*, 389, 1383
- Lammer, H., Odert, P., Leitzinger, M., et al. 2009, *A&A*, 506, 399
- Lanza, A. F. 2010, *A&A*, 512, A77
- Lanza, A. F., Aigrain, S., Messina, S., et al. 2009a, *ArXiv e-prints*
- Lanza, A. F., Bonomo, A. S., Moutou, C., et al. 2010, *ArXiv e-prints*
- Lanza, A. F., Pagano, I., Leto, G., et al. 2009b, *A&A*, 493, 193
- Leconte, J., Baraffe, I., Chabrier, G., Barman, T., & Levrard, B. 2009, *A&A*, 506, 385
- Léger, A., Rouan, D., Schneider, J., et al. 2009, *A&A*, 506, 287
- Mandel, K. & Agol, E. 2002, *ApJ*, 580, L171
- Mayor, M., Pepe, F., Queloz, D., et al. 2003, *The Messenger*, 114, 20
- Meléndez, J., Asplund, M., Gustafsson, B., & Yong, D. 2009a, *ApJ*, 704, L66
- Meléndez, J., Ramírez, I., Casagrande, L., et al. 2009b, *Ap&SS*, 221
- Michtchenko, T. A., Beaugé, C., & Ferraz-Mello, S. 2006, *Celestial Mechanics and Dynamical Astronomy*, 94, 411
- Mordasini, C., Alibert, Y., Benz, W., & Naef, D. 2009, *A&A*, 501, 1161
- Morel, P. & Lebreton, Y. 2008, *Ap&SS*, 316, 61
- Nordlund, A. 2009, *ArXiv e-prints*
- Noyes, R. W., Hartmann, L. W., Baliunas, S. L., Duncan, D. K., & Vaughan, A. H. 1984, *ApJ*, 279, 763
- Pinheiro da Silva, L., Rolland, G., Lapeyrere, V., & Auvergne, M. 2008, *MNRAS*, 384, 1337
- Press, W. H., Teukolsky, S. A., Vetterling, W. T., & Flannery, B. P. 2002, *Numerical Recipes in C++*, 2nd edn. (Cambridge University Press)
- Queloz, D., Bouchy, F., Moutou, C., et al. 2009, *A&A*, 506, 303
- Ramírez, I., Meléndez, J., & Asplund, M. 2009, *A&A*, 508, L17
- Sato, B., Fischer, D. A., Henry, G. W., et al. 2005, *ApJ*, 633, 465
- Seager, S. & Mallén-Ornelas, G. 2003, *ApJ*, 585, 1038
- Sestito, P. & Randich, S. 2005, *A&A*, 442, 615
- Siess, L. 2006, *A&A*, 448, 717
- Sing, D. K. 2010, *A&A*, 510, A21
- Snellen, I. A. G., de Mooij, E. J. W., & Albrecht, S. 2009, *Nature*, 459, 543
- Snellen, I. A. G., de Mooij, E. J. W., & Burrows, A. 2010, *A&A*, 513, A76
- Surace, C., Alonso, R., Barge, P., et al. 2008, in *Presented at the Society of Photo-Optical Instrumentation Engineers (SPIE) Conference, Vol. 7019, Society of Photo-Optical Instrumentation Engineers (SPIE) Conference Series*
- Torres, G., Winn, J. N., & Holman, M. J. 2008, *ApJ*, 677, 1324
- Winn, J. N., Holman, M. J., Henry, G. W., et al. 2009, *ApJ*, 693, 794

- ¹ Institute of Planetary Research, German Aerospace Center, Rutherfordstrasse 2, 12489 Berlin, Germany
- ² LUTH, Observatoire de Paris, UMR 8102 CNRS, Université Paris Diderot; 5 place Jules Janssen, 92195 Meudon, France
- ³ LESIA, Observatoire de Paris, Place Jules Janssen, 92195 Meudon cedex, France
- ⁴ Institut d’Astrophysique Spatiale, Université Paris XI, F-91405 Orsay, France
- ⁵ Institut d’Astrophysique de Paris, UMR 7095 CNRS, Université Pierre & Marie Curie, 98bis boulevard Arago, 75014 Paris, France”
- ⁶ Department of Physics, Denys Wilkinson Building Keble Road, Oxford, OX1 3RH
- ⁷ Observatoire de l’Université de Genève, 51 chemin des Maillettes, 1290 Sauverny, Switzerland
- ⁸ Instituto de Astrofísica de Canarias, E-38205 La Laguna, Tenerife, Spain
- ⁹ Laboratoire d’Astrophysique de Marseille, 38 rue Frédéric Joliot-Curie, 13388 Marseille cedex 13, France
- ¹⁰ Observatoire de Haute Provence, 04670 Saint Michel l’Observatoire, France
- ¹¹ Rheinisches Institut für Umweltforschung an der Universität zu Köln, Aachener Strasse 209, 50931, Germany
- ¹² Research and Scientific Support Department, ESTEC/ESA, PO Box 299, 2200 AG Noordwijk, The Netherlands
- ¹³ University of Vienna, Institute of Astronomy, Türkenschanzstr. 17, A-1180 Vienna, Austria
- ¹⁴ IAG-Universidade de Sao Paulo, Brasil
- ¹⁵ Thüringer Landessternwarte, Sternwarte 5, Tautenburg 5, D-07778 Tautenburg, Germany
- ¹⁶ Université de Nice-Sophia Antipolis, CNRS UMR 6202, Observatoire de la Côte d’Azur, BP 4229, 06304 Nice Cedex 4, France
- ¹⁷ University of Liège, Allée du 6 août 17, Sart Tilman, Liège 1, Belgium
- ¹⁸ Space Research Institute, Austrian Academy of Science, Schmiedlstr. 6, A-8042 Graz, Austria
- ¹⁹ School of Physics and Astronomy, Raymond and Beverly Sackler Faculty of Exact Sciences, Tel Aviv University, Tel Aviv, Israel
- ²⁰ Center for Astronomy and Astrophysics, TU Berlin, Hardenbergstr. 36, 10623 Berlin, Germany